To be submitted to JPO, fall 2008

Persistent Wave Groups

Jerome A. Smith
Scripps Institution of Oceanography, La Jolla, CA 92093 USA

Coralie Brulefert
Institut des Sciences de l'Ingénieur Toulon Var, Toulon, FR

ABSTRACT

During the near-field leg of the Hawaiian Ocean Mixing Experiment (HOME-NF), short steep wave groups were observed that elicited strong Eulerian responses in the observed surface current field, as reported by Smith (2006). Some of these wave groups were seen to persist for over 14 wave periods, yet were only about one wavelength long in the along-wind direction. Here we consider the evolution of wave groups of the form observed, and find that this persistence is consistent with linear dispersion in spite of the extremely compact form. The key aspects of these groups are (1) the wave crests within the group are oriented at an angle with respect to the group envelope, and (2) they are much wider in the cross-wind direction than along-wind (about 5 times). Groups with the observed 5-to-1 aspect ratio and this "slant-wave" structure can persist for up to 18 wave periods, consistent with the observations.

1. Introduction

Motivation for this work comes indirectly from the observed large responses to passing wave groups reported by Smith (2006a). In addition to the larger-than-expected response, it was noted that the wave groups responsible for inducing the response were both short, of order one wavelength, and persistent, lasting sometimes for more than 10 wave periods. Smith (2006a) focused on the Eulerian response to the groups in terms of the theory of Longuet-Higgins and Stewart (1962) and Smith (2006b), deferring examination of the wave group structure and evolution itself. Here we focus on these persistent wave groups, examining both the spatial structure and temporal evolution.

The data considered here were collected with a "Long-Range Phased-Array Doppler Sonar" (LRPADS) deployed as part of the near-field leg of the Hawaiian Ocean Mixing Experiment (HOME-NF) in the fall of 2002. This provides essentially continuous coverage of the radial horizontal surface velocity component over an area some 1500m radius by 44° azimuth, with samples every 2.5 s, every 7.5 m in range, and every 1.3° in azimuth.

The continuous 3-D coverage (2 space and time) permit fairly clean separation of the observed variability into different dynamical phenomena by various methods (Smith 2002, 2008). The approach taken here is to separate phenomena by phase speed. Surface waves are the fastest modes measured, and so can be easily separated from embedded flow features such as Langmuir circulation, fronts, or the Eulerian response to passing wave groups. After this separation, the well-constrained characteristics of surface gravity waves permit the directional response of the LRPADS to be largely compensated for, so that the surface wave propagation and evolution can be considered independently from the position across the detection area.

First we briefly review the experimental setting and operation of the instruments. Then we show an example of a compact persistent wave group which lasts for over 100 s (about 14 wave periods). We next show that linear propagation is sufficient to explain the persistence, given the actual surface wave field at a nominal starting time, and using just linear dispersion to "forward propagate" the field in time. The comparison with the later observed field is quite good. We then develop a simple model of a wave group with waves that are slanted with respect to the group envelope, and explain the persistence as a consequence of this simple structure. In contrast to previous work on modulational instabilities leading to wave group formation (e.g., Longuet-Higgins 1978; Dysthe 1979), here we are interested simply in the expected length of time wave groups of the form observed should persist.

In the discussion section, we return to the group-forced response as a convenient proxy for the occurrence of such short, steep, persistent wave groups to assess how common they were over several days (9) surrounding the observational segment shown here. The results indicate they are common, with typically 2 to 3 groups per 8.5 minute segment, whenever (but only when) the wind blows.

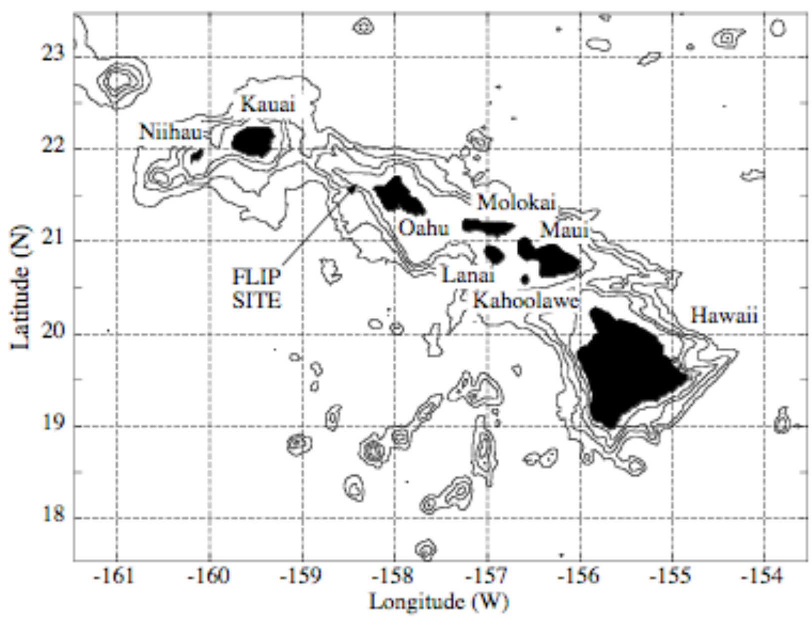

Figure 1. Location of Research Platform FLIP (Floating Instrument Platform) during the near-field leg of the Hawaii Ocean Mixing Experiment (HOME-NF), September and October 2002. The site is about 30 km West of Oahu, over an underwater ridge that extends roughly halfway to Kauai. Depth contour interval is 1000 m, deepest shown is 4000 m. (Figure from Smith 2006a.)

2. Experimental Setting and Data

Quantitative estimation of the directional surface wave field requires data that are extensive in both time and space: direction, wavelength, and frequency must be resolved over a wide range of scales. To provide this, a 50-kHz "Long-Range PADS" (LRPADS) was operated continuously for about 20 days, from 14 September to 5 October 2002. The data were gathered aboard the Research Platform (R/P) Floating Instrument Platform (FLIP), in conjunction with the HOME-NF, at a location just West of Oahu (figure 1). The general design and operation of a "Phased-

Array Doppler Sonar" (PADS) is described in Smith (2002) and extension to the "Long-Range" version (LRPADS) is summarized in Smith (2006a). The brief description here follows the latter.

To obtain velocity estimates over an area of order 1 km^2 , a 50 kHz acoustic signal is transmitted in a 44° wide fan every 2.5 seconds, with a vertical beamwidth sufficient to encounter the surface beginning a few tens of meters away, and continuing until attenuation reduces the backscattered signal level below the ambient noise. Vertical location is not resolved; the 22° vertical beam-width takes in the surface bubble layer beyond about 90 m range, and the effective location of the measurements is dictated by the centroid of these scatterers (in the frequency range considered here, 45 kHz to 55 kHz, bubbles produced by breaking waves are very efficient scatterers, typically producing some 40 dB more backscatter than all other scatterers). In the open ocean, bubbles have a mean vertical distribution that is approximately exponential, with a depth scale of order 1.5 m, depending weakly on windspeed (Thorpe 1986; Crawford and Farmer 1987). Thus the measurements can be considered as essentially surface velocities.

For the LRPADS as configured in HOME-NF, an area extending roughly 1.5 km in range and 44° in bearing is segmented into measurement bins about 1.3° wide (35 beams) and 7.5 m in range (200 range bins), a total of 7000 locations. The area is sampled every 2.5 s (the time needed for sound to propagate out 1800 m and back). The LRPADS was operated with 10 kHz sample rate (complex samples, so each sample has both amplitude and phase). With 10-kHz sample rate and 50-kHz center frequency, the "code bits" (=1 sample) correspond to about five acoustic wave cycles each. A plane wave from the outermost angles (±22°) completes 16 cycles across the face of the receiver array, corresponding to about 3 bits' worth; thus, beam forming is done via time delay. While this is more computationally demanding than FFT beam forming, it has the advantage of reducing the ambiguity between the two Nyquist wavenumber angles (+22° and -22°). As operated, the selectivity between +22° and –22° appears empirically to be on the order of 6 dB. The raw data stream was segmented into files of roughly 8.5 min each. Retaining raw data permits experimentation with new beam-forming algorithms, focusing, re-sampling with a higher range resolution, *et cetera*. The Doppler shift is estimated with a time-lagged covariance technique, treating each ping independently. This yields a finite level of Doppler noise even at a high signal-to-noise ratio (SNR); here repeat-sequence codes were used to reduce the Doppler noise (Pinkel and Smith 1992), resulting in single-ping rms noise levels of about 7 cm/s per range/angle bin (see discussion section). At the farthest ranges, the SNR decreases as the signal fades into the ambient acoustic noise, further degrading the estimates. Here we taper the data to zero to facilitate FFT procession, stopping well short of ranges where the ambient noise is an issue, even when ships or other noise sources are present. This provides both the surface waves and the underlying surface flows over a suitable area, with the requisite continuous coverage in both space and time.

In addition to the LRPADS data, many other measurements were made from R/P FLIP. These include wind, surface wave elevation spectra, and rapid-profiling "CTD" profiles ("Conductivity, Temperature, and Depth," with which salinity and density can be calculated) every 4 minutes or so throughout HOME-NF (e.g., see Pinkel and Rudnick 2006; Klymak et al. 2008).

3. Observed Persistent Wave Groups

As noted, the surprisingly prominent Eulerian response to passing groups provided the initial motivation to consider the waves in this data set. Here, we focus on the wave groups themselves. Specifically, we consider the linear dynamics and evolution of the wave groups as observed, which can be quite short in the along-wave direction (about 1 wavelength), yet remarkably persistent, having been observed to last more than 14 wave periods in a few cases. We begin by considering a particular example in some detail. Later we will evaluate how representative this example is.

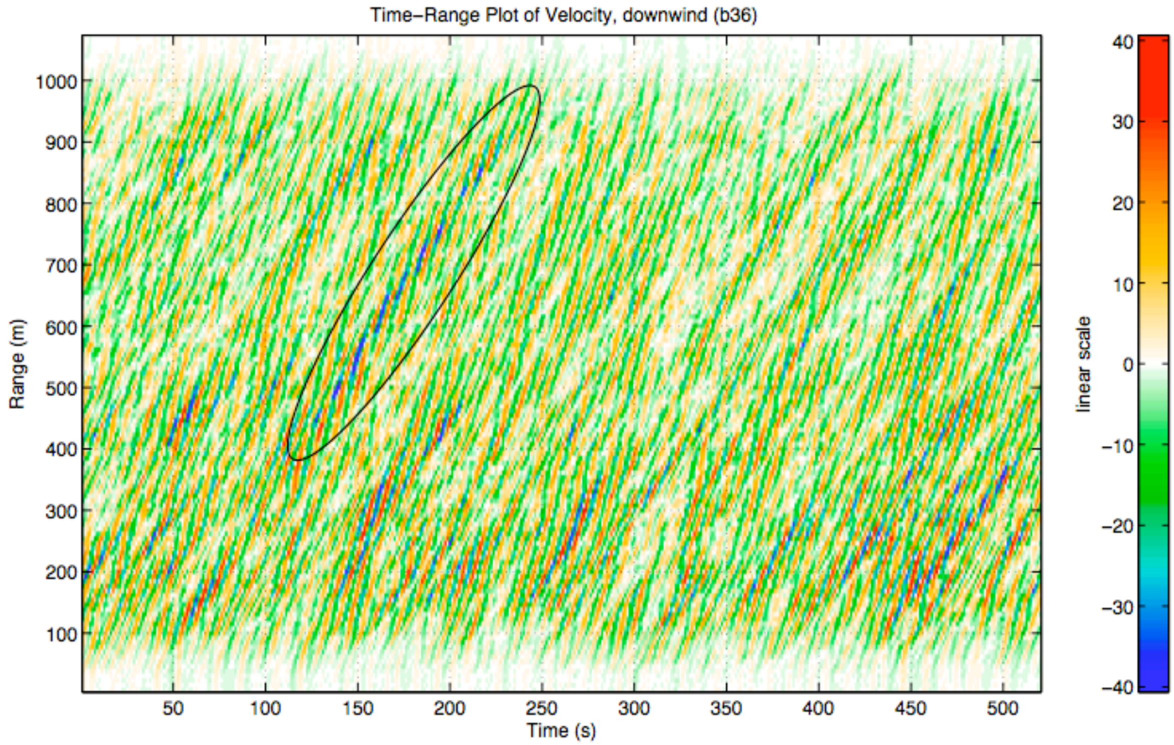

Figure 2 An example time-range plot of radial surface velocity along a single sonar beam. Note the appearance of wave groups (groups of higher amplitude waves), such as the one circled.

A useful and revealing way to view wave propagation is via contours of velocity plotted on a time-range plane (a "T-R plot"), as in Figure 2. Distinct wave groups appear as diagonal "slashes" of higher-amplitude velocities, within which the phase velocity can be perceived as the more steeply angled crests and troughs of the waves. The group circled in Figure 2 can be seen to persist for about 100 s. Since the waves comprising the group have about a 7 s period, this corresponds to about 14 wave periods.

In the full three-dimensional view, the spectrum of waves has several peaks in direction and frequency, some of which confuse the picture yet don't interact with the wave groups of interest here. For clarity, the data in figure 2 were filtered for outgoing waves only, suppressing some large upwind-propagating swell.

Fourier Transform Processing – Time-Range to Frequency-Wavenumber

An FFT (Fast Fourier Transform) in time yields both positive and negative frequencies that are complex conjugates of each other, and so redundant. The FFT can be used to generate an imaginary component of the original times-series by setting all negative frequencies to zero, increasing the positive frequency coefficients by the factor $2^{1/2}$ (to preserve the variance), and then doing the inverse transform. The result yields both the original series as the real part and a Hilbert transform as the imaginary part. This synthesized imaginary part effectively incorporates temporal information into each spatial "snapshot," so the direction of propagation of each wavenumber component is unambiguous. This permits each spatial snapshot to be processed independently, with no ambiguity in direction as occurs with only the original (all real) spatial snapshot (described further below).

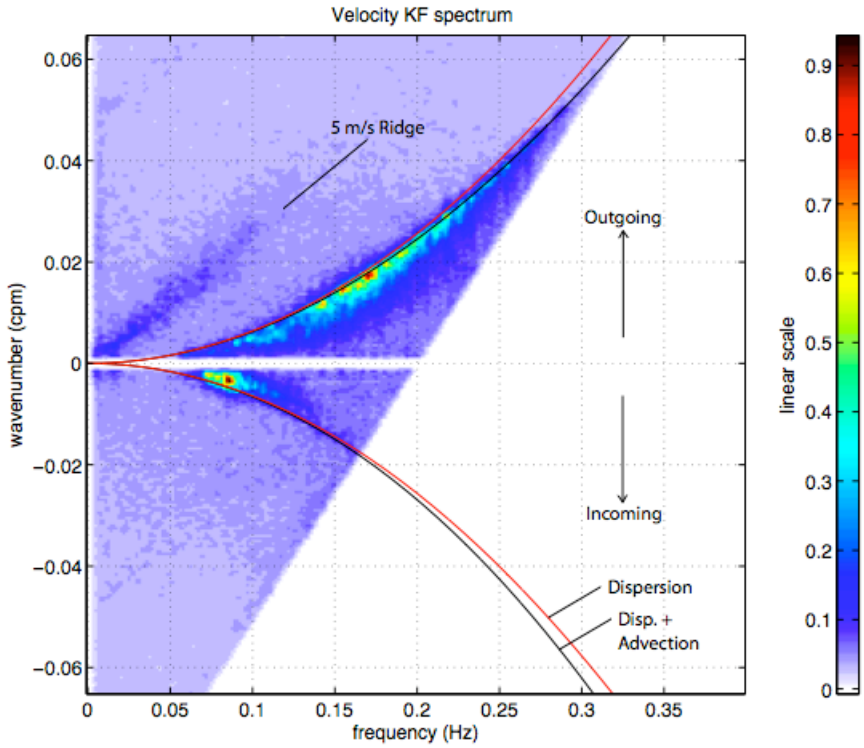

Figure 3. A typical wavenumber-frequency *(k-f)* spectrum from the LRPADS surface wave data set. Note the straight ridge of variance at a slope corresponding to 5 m/s, and the surface-wave related ridge which is roughly a quadratic in *f*. The red curves correspond to linear dispersion, while the black curves are corrected for advection by the observed mean current. The outgoing waves go more nearly downwind, so the wave variance is generally larger on that half of the spectrum. The bottom half was zeroed to make Figure 2.

Working from the temporal FFT (frequency) data, a spatial FFT can then be performed, using a finite range interval of dependably good data, which we take here as about 100 to 950 m (this rather short end point insures that the signal will dominate even over the occasional noisy boat traffic). The result is a two-dimensional (2-D) Fourier transform from time and range to frequency and wavenumber (Figure 3). A notable feature of this 2-D spectrum is that the upper half (outgoing waves) has a much larger area of high wave energy; these correspond to approximately downwind-traveling waves.

As is clear from looking at the *k-f* spectrum (Figure 3), the branch of wave energy in the upper half extending past the Nyquist frequency of 0.2 Hz corresponds to genuine, but higher frequency, waves (the Nyquist frequency is that for which there are 2 samples per cycle; with 2.5 seconds per sample, the Nyquist frequency is 1/5 s = 0.2 Hz). We know the higher frequency waves propagate predominantly downwind, so the inherent ambiguity of location of a given portion of variance on the *k-f* plane between (+frequency, +wavenumber) versus (–frequency, –wavenumber) can be resolved to favor downwind traveling components. This permits examination of wave components with frequencies higher than the Nyquist frequency of 0.2 Hz.

In the present analysis, we are concerned about waves with periods of order 7 s, so this is an aside. To recover these waves back in time-range space, we would need to synthesize a time-series with more samples in time. This can be achieved by cutting the *k-f* plane at an angle, cutting out the upwind-traveling "false aliases" but retaining the "true aliased" energy along the downwind wave ridge to higher frequencies. Then, to interpolate to twice the sample rate while retaining this variance, we would extend the zeroed area along the frequency axis to twice the original Nyquist frequency. The resulting inverse Fourier transformed data would have samples every 1.25s (twice as often), and the waves above 0.2 Hz would appear to propagate downwind as they should. In practice, it appears we could examine waves in this way up to 0.3 Hz or more.

Correcting for the directional response of the array

Each sonar beam detects just the radial component of the surface velocity. For the geometry of deployment in HOME-NF, this corresponds to a horizontal component of the orbital velocities of the waves, sampled along a line at the surface every 7.5 m (from about 100 to 1500 m in range) and every 2.5 s (continuously, but broken into 8.5 minute files). The response to waves propagating at an angle θ to the wind is reduced by $\cos\theta$ compared to the waves traveling straight along the beam either towards or away from FLIP. To get a complete estimate of wave elevations, for example, we wish to correct for this to the degree possible. Here we outline a method to apply a partial correction using a wavenumber-frequency transform of the time-range data from a single beam at a time. The method is essentially as described by Smith (2006a), with a minor modification.

We begin with the 2-D frequency-wavenumber transform from the time-range data of a single beam at a time, as described above. The components $U(f, k_r)$ are the Fourier coefficients from the time-range Fourier transforms of the radial velocities $u(t, r)$ along a given sonar beam. Then, in the surface-wave part of the spectrum, at each frequency f the radial wavenumber component is $k_r = k\cos\theta$, where $k = k(f)$ is the magnitude of the total wavenumber, which can be obtained from the linear dispersion relation. In the presence of a mean current, the deep-water linear dispersion equation for surface gravity waves is

$$\omega = (g\kappa)^{1/2} + \kappa V\cos(\theta_k - \theta_V) \tag{4.1a}$$

or

$$f = (gk/2\pi)^{1/2} + kV\cos(\theta_k - \theta_V) \tag{4.1b}$$

where f is the wave frequency in Hz (or ω in rad/s), k the wavenumber in cycles per meter (cpm; or κ in rad/m), θ_k is the direction of the wave and θ_V is the direction of the current. This can be solved for $k(f)$ in a form that is well behaved as $V \to 0$ (Smith and Bullard 1995):

$$k(f) = (8\pi g^{-1})f^2\left(1 + \left\{1 + (8\pi g^{-1})fV\cos(\theta_k - \theta_V)\right\}^{1/2}\right)^{-2}. \tag{4.2}$$

In general, the currents are small compared to the wave phase speeds. For example, a 3 s wave has a phase speed $c = \omega g^{-1} = 2\pi f g^{-1}$ of about 4.7 m/s, while the typical currents are 0.20 m/s or less, so $V/c \approx 0.04$. In terms of the small normalized current $\hat{V} \equiv V/c$, 4.2 simplifies to roughly

$$k(f) \approx k_0\left(1 - 2\hat{V}\cos(\theta_k - \theta_V)\right). \tag{4.3}$$

where k_0 = $(2\pi g^{-1})f$ is the zero-current value for k. Although this correction is small, it is large enough to see on the k-f spectral plots (see figure 3). It is also cumulative, and so becomes noticeable after the waves propagate for 100 s or so, as we hope to test here.

To derive (for example) the elevations from the radial component of velocities $U_r = U\cos\theta$, the measured component U_r should first be divided by the response $\cos\theta = k_r/k$; however, this is singular near the k_r=0 axis. In Smith (2006a) a weighting function was introduced to prevent this singularity. Here, we use an analogous weighting, but make a slight improvement by forming an optimal estimate of $U_r/\cos\theta$ in the presence of noise. Let the observed velocity be the sum of the true value plus a uniform variance, zero-mean noise term "ε":

$$U_0 = U(f,k_r)\cos\theta + \varepsilon = 2\pi f\ A(f,k_r)\,(k_r/k_f) + \varepsilon \tag{4.4}$$

where k_f is the wavenumber magnitude from dispersion, k_r is the component as measured along the sonar beam under consideration, θ is the angle between the beam direction and the wave propagation direction, and $A(f,k_r)$ is the elevation amplitude of the component with frequency f and along-beam wavenumber k_r. Then we seek an optimal weight "b" so that the estimate $\hat{U} \equiv bU(f,k)$ has minimal error relative to the "true U" (which is in direction of wave propagation at the crests):

$$\left\langle \left|\hat{U} - U\right|^2 \right\rangle = \left\langle \hat{U}^2 \right\rangle - 2\left\langle \hat{U}U \right\rangle + \left\langle U^2 \right\rangle = \text{minimum} \tag{4.5}$$

Differentiating with respect to b and setting the result to zero yields

$$b = \frac{q}{q^2 + <\varepsilon^2>/<U^2>} \tag{4.6}$$

where $q = \cos\theta = k_r/k_f$. The velocity variance $<U^2>$ is related to the elevation variance as $U^2 = \omega^2 A^2(f) = (2\pi f)^2 A^2(f)$, so if the elevation frequency spectrum has the form $<A^2(f)> \propto f^{-5}$ then $<U^2> \propto f^{-3}$. To avoid specifying both the waves' orbital variance and the noise level explicitly, we instead specify a "critical frequency" f_C at which $\varepsilon^2 = U^2(f_C)$. Then, since we know $<U^2> \propto f^{-3}$, it follows that $<\varepsilon^2>/<U^2> = (f/f_C)^3$. We estimate the critical frequency by observing where the surface-wave related ridge on the measured k-f spectrum fades into the background. For example, on the upper (downwind) branch in figure 3, this appears to occur near f = .32 Hz. In terms of the critical frequency, the optimal weight is

$$b = \frac{q}{q^2 + (f/f_C)^3}\,. \tag{4.7}$$

Although each individual beam is "blind" to waves incident at a right angle to the beam direction, the beam directions over the whole field of view cover about 44°, so the array taken together can detect waves going in any direction to some degree.

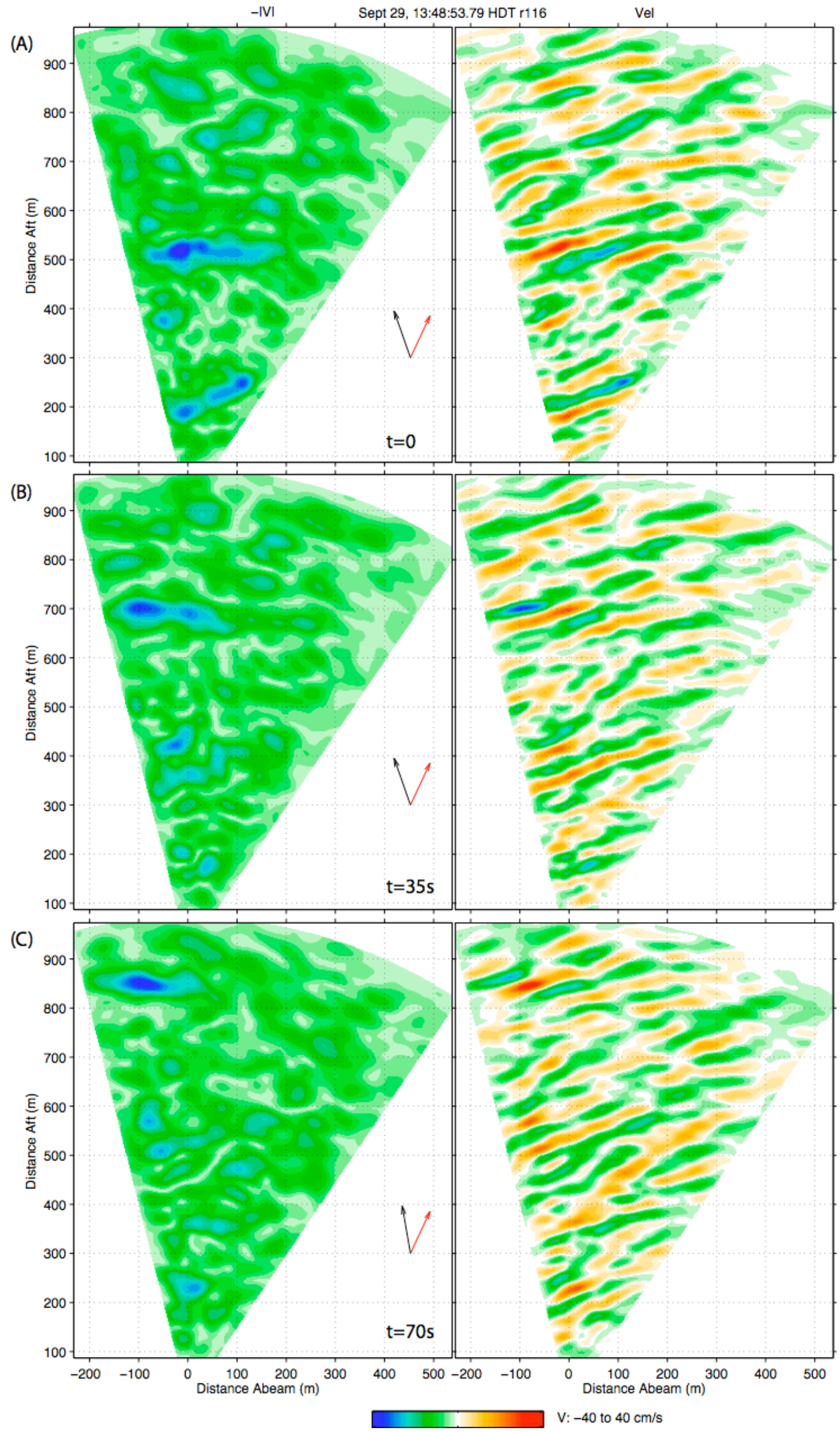

Figure 4. A series of frames showing wave propagation. Each panel shows (left) the amplitude envelope of the waves (plotted negative for a better color match) and (right) the actual surface velocity field. (Top) a good "initial frame," this shows both a "slant-wave group" (near 500 m range) and a "standard wave group" (near 200 m). Note that the wave crests (right) in the lower group are nearly parallel to the envelope (left panel), while the upper group has crests slanted at an angle with respect to the envelope orientation. (Middle) The fields 35 s later (5 wave periods). Here the lower group has already dispersed, while the upper group continues. (Bottom) Even after 70s (10 wave periods), the slant-wave group persists.

A useful way to characterize the resulting directional response is to specify where the practical weight *"b"* is just half as large as the ideal weight $1/q = 1/\cos\theta$. This is just where $½ = bq = q^2/(q^2+(f/f_C)^3)$, or $q = (f/f_C)^{3/2}$. For example, with $f_C = 0.32$ Hz, the 7-second-period group waves have a critical-frequency ratio f/f_C of about $1/2.25 = (1/1.5)^2$, so the response is half as large as ideal at $q = (1.5)^{-3}$ or for θ about 17° short of 90°. At this frequency, then, waves propagating within 73° of parallel to the axis of the pie have at least half the beams with a response factor of better than ½. Here, the focus is on waves and groups propagating downwind, and hence on waves going within 45° to 60° of being directed along the axis of the pie. Thus, for this study no additional correction is applied beyond the above described optimal weight.

The optimal weights can be defined and evaluated separately for the waves propagating away (k_r positive) versus towards FLIP (k_r negative). This permits choosing different values of f_C for downwind versus upwind waves. Also, note that the sign of approaching waves' orbital velocities are reversed (in accordance with k_r being negative), so in all cases the estimated $\hat{U}$ corresponds to the velocity at the crest being directed towards the estimated true wavenumber direction. Thus, for example, dividing the estimated $U(f,k_r)$ by the corresponding frequency $2\pi f$ (from dispersion) results in proper estimates of elevation $\zeta(f,k_r)$.

Figure 4 shows some example velocity fields corrected for the directional response, with the actual velocity field on the right and the amplitude (velocity envelope) on the left.

5. Linear Propagation Model

As noted, the implementation of the "positive frequency only" FFT processing incorporates directional propagation information implicitly into the spatial maps of (complex) velocity in each frame (or time sample). Thus the 2-D spatial map of complex velocities can be processed independently for each ping, or time sample, without any directional ambiguity.

The simplest model for wave evolution is based on linear propagation of each wavenumber component, with sinusoidal behavior in both time and space, and the temporal dependency (frequency) deduced via linear dispersion from the wavenumber, which is derived from a spatial 2-D FFT of the velocity field. As before, the area-mean current can be incorporated in the dispersion relation for $f(k)$ (equation 4.1b). Although this correction is small, it can have a noticeable effect over the 100 s life-span of the wave groups: a 20 cm/s current would result in a 20 m offset after 100 s, a significant fraction of the order-70 m group length.

To implement the linear propagation model, we start with any specified snapshot (at a time designated t_0), take the 2-D spatial FFT, and propagate each component forward in time by multiplying each complex wavenumber component by the corresponding factor $\exp(-i2\pi f(k)(t-t_0))$. We then compare the evolution of the observed velocity field with the one derived from the initial snapshot as propagated forward in time by this linear model. Figure 5 shows both the linearly-propagated velocity fields and the observed velocity fields, while Figure 6 shows the corresponding wave envelopes, all as propagated from the initial time shown in the top panel of Figure 4. Comparing only the ever-smaller area where the linear propagation model has a fair chance (i.e., ever more to the upper left corner, since zeroes are propagating in from the bottom and right), it is seen that the velocity variance matches to better than 10% even after 10 wave periods (70s).

In both the real data and the linear propagation model, we observe that there are two kinds of wave groups:

- One kind of group (seen near 200m range at the bottom of the pie in figure 4) disperses quickly. The waves inside the group are aligned with the envelope (i.e., the crests are roughly parallel to the main axis of the envelope).

- The other kind of group (starting near 500m range in figure 4) has an envelope narrow in "x" (vertical) and broad in "y" (left to right), but has waves inside that propagate at some angle θ with respect to the group envelope orientation.

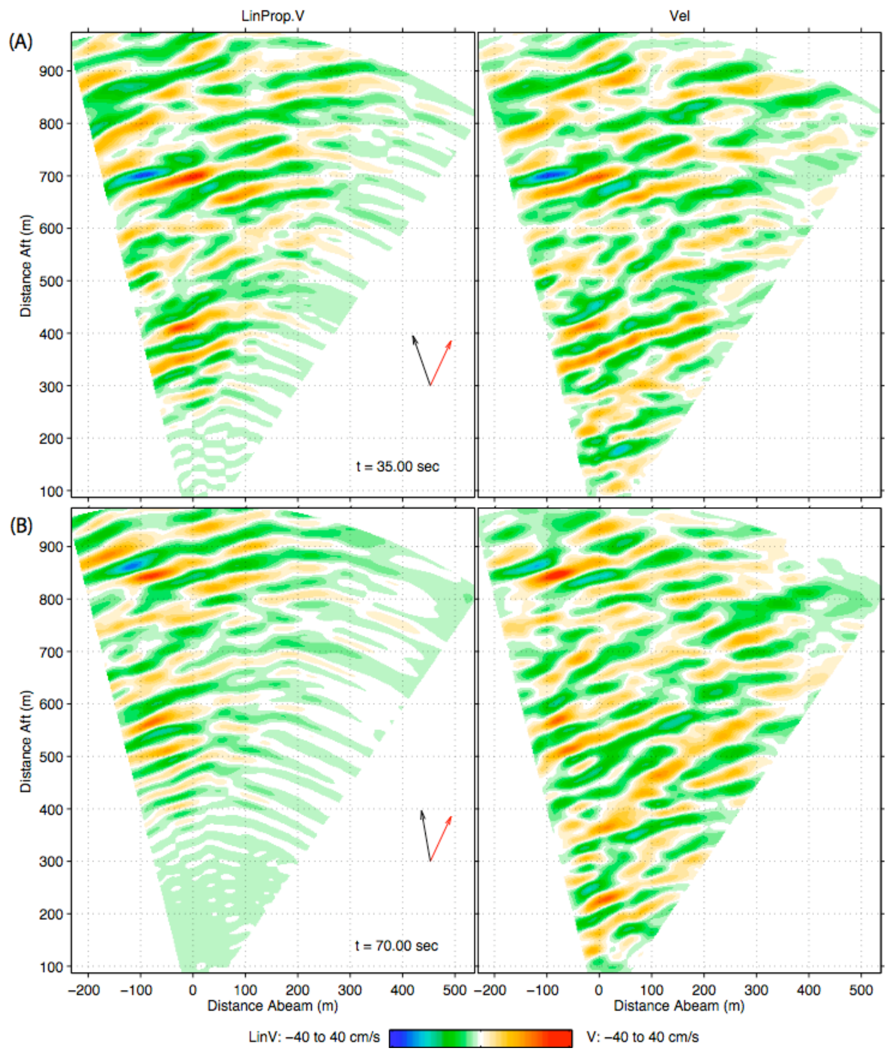

Figure 5: Comparison between linear propagation (left) and the real (observed) propagation (right) after 5 wave periods (upper panel) and 10 wave periods (lower panel). The initial snapshot is shown in Figure 4a (top). The model looks like the real data in the upper left area, following the propagating persistent wave group. The lower right edge of the pie becomes small in the linear-propagation model as zero-amplitude waves propagate into the field of view through the boundary.

We focus on the group which doesn't break up, the "persistent wave group." What accounts for the endurance of this group? There are three kinds of explanations: (1) superposition of independent wave components obeying linear dispersion, but with waves that are slanted at an angle with respect to the group envelope (a "slant-wave group"); (2) nonlinear dispersion and wave-wave interactions; and (3) advection by the underlying forced response. As seen in figures 5 and 6, the difference between the linearly propagated velocity field and the observed velocity field is small (of order 10% or less), and the propagated wave group envelope remains as tight as the observed one, indicating that linear dynamics are sufficient to explain these short, steep, yet persistent wave groups. Explanation (1) is the simplest, and also fits the data as indicated by the linear propagation model comparison, so it is preferred. As an aside, it is worth noting that the nonlinear dispersion correction and advection by the forced group response have opposing tendencies, and so at least partially cancel. This may help explain why linear dispersion works so well, even after times long enough to see very subtle errors in propagation speed.

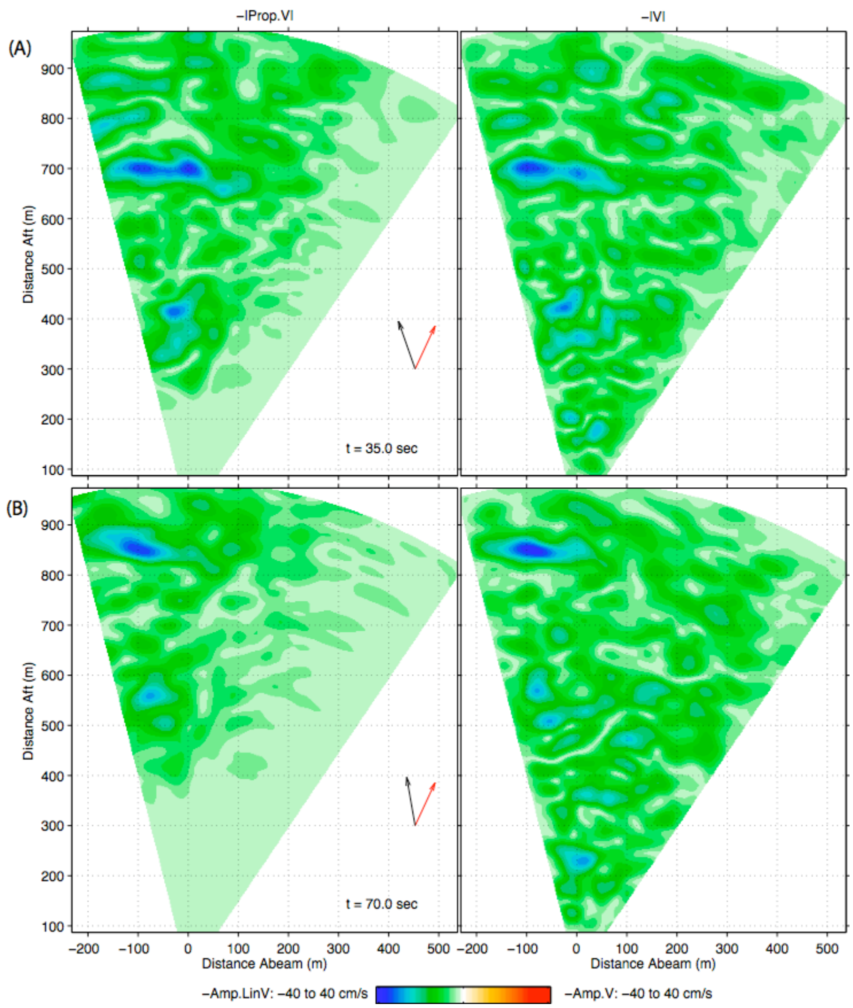

Figure 6: As in figure 5, but showing the velocity amplitude envelopes. The linear propagation results (left) and observed waves (right) after 5 (upper) and 10 (lower) wave periods show good agreement in the area where the propagation has a fair chance. The initial snapshot is shown in Figure 4a (top) on the left.

We next use some characteristic values of the persistent group to examine and understand its behavior.

6. Group Evolution and Dispersion

Now we consider the linear propagation of a model wave group in which the waves comprising the group are at an angle θ relative to the group envelope orientation – a "slant-wave group."

To help fix ideas, first consider a simple sum of 2 waves of amplitudes a and b (e.g., for elevation), and with slightly different values of the x-component of wavenumber k and the corresponding difference in frequencies ω (but no difference in the y-component of k):

$$\begin{aligned}\zeta(x,y,t) &= \mathrm{Re}\{ae^{i(kx+ly-\omega t)} + be^{i((k+\Delta k)x+ly-(\omega+\Delta\omega)t)}\} \\ &= \mathrm{Re}\{ae^{i(kx+ly-\omega t)}[1+(b/a)e^{i(\Delta kx-\Delta\omega t)}]\}\end{aligned} \tag{6.1}$$

Expanding $\Delta\omega \approx \Delta k_x(\partial\omega/\partial k_x) = \Delta k_x c_x^g$, the envelope factor on the second line is seen to propagate at $c_x^g \equiv \partial\omega/\partial k_x$:

$$[1+(b/a)e^{i(\Delta kx-\Delta\omega t)}] \approx [1+(b/a)e^{i\Delta k(x-c_x^g t)}] \tag{6.2}$$

Since the observed envelope is much narrower in x than y, we know the wavenumber spread must be dominated by Δk_x, as in this simple superposition example. Even if the waves comprising the group are oriented at some angle to the x-axis, the group envelope is long in y and short in x, and its major axis is roughly parallel to the y-axis, so $\Delta k_x >> \Delta k_y$.

What is observed in the data (see Figure 4) is a wave group envelope which propagates at about 5 m/s in the x-direction (vertical in figures 4 through 6). In these figures, the pie-plots were rotated so the persistent wave group's envelope is oriented with the short dimension in x. The group length in this direction is about 70 m, or about 1 wavelength at the center wave-period of about 7 s, and is initially about 5 times that in the y-direction.

We shall start with a specified wave group and estimate how quickly it disperses with time. It's useful to first define and examine a curve on the wavenumber plane showing all waves that have an x-component of group velocity c_x^g matching the observed group propagation speed in that direction. Figure 7 shows the 2-D wavenumber spectrum corresponding to the data shown in figure 4 for an area immediately surrounding the persistent wave group (400m by 400m centered on the group), with a roughly oval curve showing the locus of wavenumber components for which c_x^g = 5 m/s. The center wavenumber of the group is assumed to lie on this curve. The spread in wavenumber is assumed to be dominated by Δk_x. In general, if the center wavenumber is not pointed along the x direction, the wave components comprising the group will have a finite spread in both length and direction. To set the values of Δk_x and Δk_y, we use length-scales estimated from Figure 4:

$$\Delta k_x, = 2\pi/L_x \text{ and } \Delta k_y, = 2\pi/L_y, \tag{6.3}$$

where $L_x \approx 70$ m and $L_y \approx 5L_x \approx 350$ m.

Since the x-wise width of the group envelope is roughly a wavelength, it follows that $\Delta k_x \approx |k|$. The spread of peaks in the x-direction in the actual estimated 2-D wavenumber spectrum (Figure 7) is consistent with this.

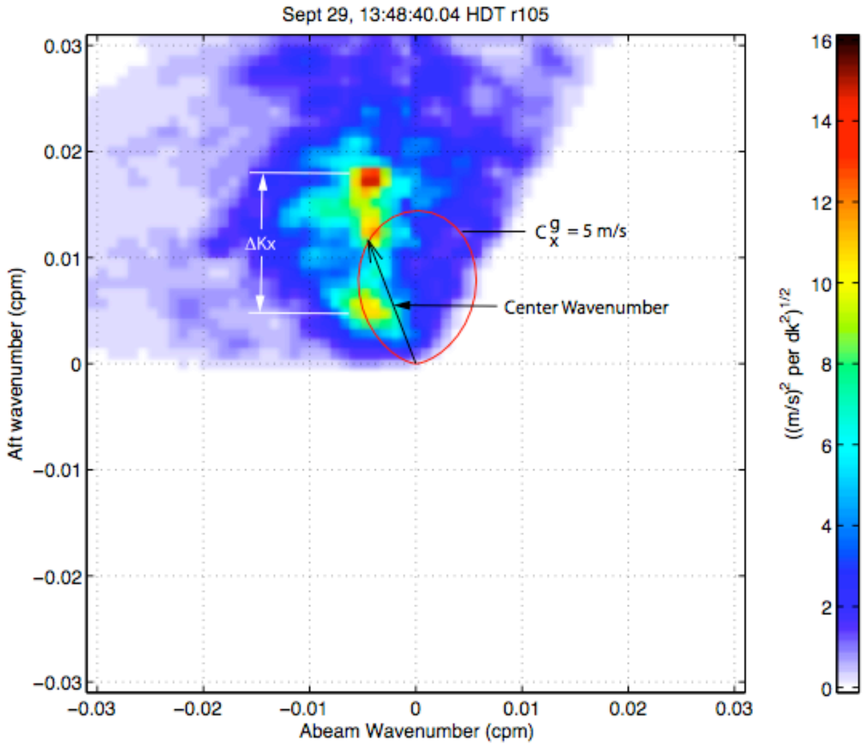

Figure 7: A 2-D wavenumber spectrum corresponding to the times illustrated in figure 4, but focusing on the persistent group (using a box 400m on a side centered on the group in each frame and averaged). The roughly oval curve shows all waves that have a group velocity component in the *x*-direction of 5 m/s. The orientation of the LRPADS image has been rotated so the short dimension of the group is aligned with *x* (upwards). Also shown schematically is a nominal "center wavenumber" and a Δk_x corresponding to the spread over the three visible peaks.

To estimate a group dispersal time, we estimate how long it should take for the area of the group to spread out to twice the initial area from an initially compact form. This is taken as roughly the time it takes the spread in component group velocities to separate the components by a distance L_x or L_y. We begin by defining just the "*x*-wise" and "*y*-wise" dispersion times:

$$T_x = \frac{L_x}{\left|\Delta c_x^g\right|} \text{ and } T_y = \frac{L_y}{\left|\Delta c_y^g\right|} \qquad (6.4)$$

To obtain the spread in component group velocities Δc_x^g and Δc_y^g, we assume that the main cause of this spread is the spread Δk_x in k_x. From expansions in $k + \Delta k$ about the center value c_{x0}^g:

$$c_x^g \approx c_{x0}^g + \Delta k_x \frac{\partial c_x^g}{\partial k_x} \text{ and } c_y^g \approx c_{y0}^g + \Delta k_x \frac{\partial c_y^g}{\partial k_x} \qquad (6.5)$$

where the partial derivatives are evaluated at the center wavenumber (and hence on the "5 m/s curve"). Thus we need the partial dependencies of the two components of group velocity on just the *x*-component of wavenumber, $\partial c_x^g / \partial k_x$ and $\partial c_y^g / \partial k_x$:

$$\frac{\partial c_x^g}{\partial k_x} = \tfrac{1}{2} g^{1/2} \frac{\partial}{\partial k_x}\left(\frac{k_x}{(k_x^2 + k_y^2)^{3/4}}\right) = \frac{c^g}{k}\left(1 - \frac{3}{2}\cos^2\theta\right) \tag{6.6a}$$

and

$$\frac{\partial c_y^g}{\partial k_x} = -\frac{c^g}{k}\left(\frac{3}{2}\sin\theta\cos\theta\right) \tag{6.6b}$$

Now we re-cast these in terms of just the observed x-wise group speed $V \approx 5$ m/s (defined as fixed) and the center component angle θ. The angle of propagation θ is defined as usual for the choice of axes: 0° is upwards (parallel to the x-axis), with positive angles increasing counter-clockwise so +90° points along the $+y$ axis. Then $c^g = V/\cos\theta$ and $k = g\cos^2\theta/4V^2$, so

$$\frac{\partial c_x^g}{\partial k_x} = \frac{4V^3}{g\cos^3\theta}\left(1 - \frac{3}{2}\cos^2\theta\right) \text{ and } \frac{\partial c_y^g}{\partial k_x} = -\frac{6V^3}{g}\left(\frac{\sin\theta}{\cos^2\theta}\right). \tag{6.7a,b}$$

To take the absolute value, we note that both are negative for $0 < \theta < 35.26°$ (here 35.26° is about where $\cos^2\theta = 2/3$), so we restrict the angles considered for the group center component to this range and reverse the signs. Then the magnitudes of group velocity spreads are

$$\left|\Delta c_x^g\right| \approx \Delta k_x \frac{4V^3}{g}\left(\frac{3}{2\cos\theta} - \frac{1}{\cos^3\theta}\right) \text{ for } |\theta| < 35.26° \tag{6.8a}$$

and

$$\left|\Delta c_y^g\right| \approx \Delta k_x \frac{6V^3\sin\theta}{g\cos^2\theta} \text{ for } 0 < \theta < 180° \tag{6.8b}$$

With the spread in group velocity components in hand, we next consider 3 simple cases, and estimate the expected duration of each kind of group: (1) where $\theta = 0°$, so the wavenumber spread is parallel to the center wavenumber; (2) where $\theta = 35.26°$, so there is only y-dispersion; and (3) a realistic case based on the observed group.

Case 1. $\theta = 0°$

In this case, there is no y-dispersion ($\Delta c_y^g = 0$), and $\cos\theta = 1$ so all the waves are colinear. Substituting the values from above, we find

$$T_D = T_x = \frac{L_x}{\left|\Delta c_x^g\right|} = \frac{gL_x^2}{4\pi V^3} \approx 31\text{ s} \tag{6.9}$$

or about 4.5 wave periods.

Case 2. $\theta \approx 35.26°$

In this case, $\Delta c_x^g \approx 0$, so the group only disperses laterally (in y). This case corresponds to a center-wave which, in a figure like Figure 7, has a wavenumber that lies at the point where the tangent to the "5 m/s curve" is vertical. At that point, $\cos^2\theta = 2/3$, and hence $\sin\theta = (1/3)^{1/2}$. Then $\Delta c_y^g \approx 2\pi 3^{3/2} V^3/gL_x$, and we find

$$T_D = T_y = \frac{L_y}{\left|\Delta c_y^g\right|} = \frac{gL_xL_y}{2\pi 3^{3/2} V^3} \approx 59 \text{ s} \tag{6.10}$$

or about 8.5 wave periods.

Case 3. Given L_x, L_y, and V, what center angle yields the most persistent group?

By inspection, the longest duration must occur approximately at the angle where $T_x = T_y$. Again we restrict consideration to $0 < \theta < 35.26°$ (to eliminate the absolute value operation, and also because we know the desired solution must lie in that range). Then we have

$$T_y = \frac{L_y}{\left|\Delta c_y^g\right|} = \frac{gL_xL_y\cos^2\theta}{6\pi V^3 \sin\theta} \approx T_x = \frac{L_x}{\left|\Delta c_x^g\right|} = \frac{gL_x^2\cos^3\theta}{4\pi V^3(1-\frac{3}{2}\cos^2\theta)}. \tag{6.11}$$

Eliminating common factors and applying trigonometric identities, the angle for which this equality holds is a solution of

$$\cos 2\theta - \frac{L_x}{L_y}\sin 2\theta - \frac{1}{3} = 0. \tag{6.12}$$

Substituting $x = \cos 2\theta$, we then also have $\sin 2\theta = (1\text{-}x^2)^{1/2}$, and this can be rearranged into a quadratic equation:

$$(1+R^2)x^2 - \tfrac{2}{3}x + (\tfrac{1}{9} - R^2) = 0 \tag{6.13}$$

or

$$\cos 2\theta = \frac{1/3 \pm \sqrt{1/9 - (1+R^2)(1/9 - R^2)}}{1+R^2} \tag{6.14}$$

where $R = L_x/L_y \approx 1/5$. The solution in our range of interest ($0 < \theta < 35.26°$) corresponds to $\theta \approx 29.8°$. The values of T_x and T_y are both about 154 s for this case; however, this time would correspond to an expansion to 4 times the area, rather than just twice. Since the area is the product of the two dimensions, and the expansion in both directions is linear in time, the area can be expressed as a function of time:

$$A(t) \approx L_xL_y(1 + t/T_x)(1 + t/T_y). \tag{6.15}$$

with $T_x = T_y = T = 154$ s, the two time-factors multiply to 2 when $t = (2^{1/2}\text{-}1)T \approx 64$ s, or about 9 wave periods, just slightly more than case 2.

In the above, the duration estimate corresponds roughly to the time it takes a "well formed" (maximally compact) group to disperse to twice the area (and hence half the energy density). Since the linear dynamics are time-reversible as posed, the time for the groups to coalesce would be exactly the same, and so the total durations of each kind of group (from dispersed to compact to dispersed again) are about twice the above values. Thus, the colinear group would endure for about 9 wave periods, while the "lateral group" would persist for 17, and the optimal slant-wave group for 18. Both cases 2 and 3 are consistent with the observed group persisting 14 periods, showing that the persistence is not strongly dependent on the internal wave angle over the range between these two cases (29.8° to 35.26°).

Note that case 3 reduces to case 2 when $L_y >> L_x$ (so R ≈ 0). This limiting case can be conceptualized as being like the wake of a boat that has moved at a constant speed in a straight line. In this case, we know the leading edge of such a wake (which makes about a 19.5° angle with respect to the boat's path) remains well-formed, with the largest wake-waves confined to a relatively narrow envelope near that leading edge. The waves within the wake can be seen to be oriented at an angle to the wake-envelope, consistent with the case 2 results. Naturally, the question arises whether the observed persistent groups are remnants of actual ship wakes. The angle of the wake to the ship-track implies a ship speed about 3 times the speed of advance of the wake in the direction orthogonal to the wake's leading edge; thus, this would require ships going 15 m/s, which is rare. The high speed and the frequency of occurrence of such groups (see discussion section) appear to rule this out.

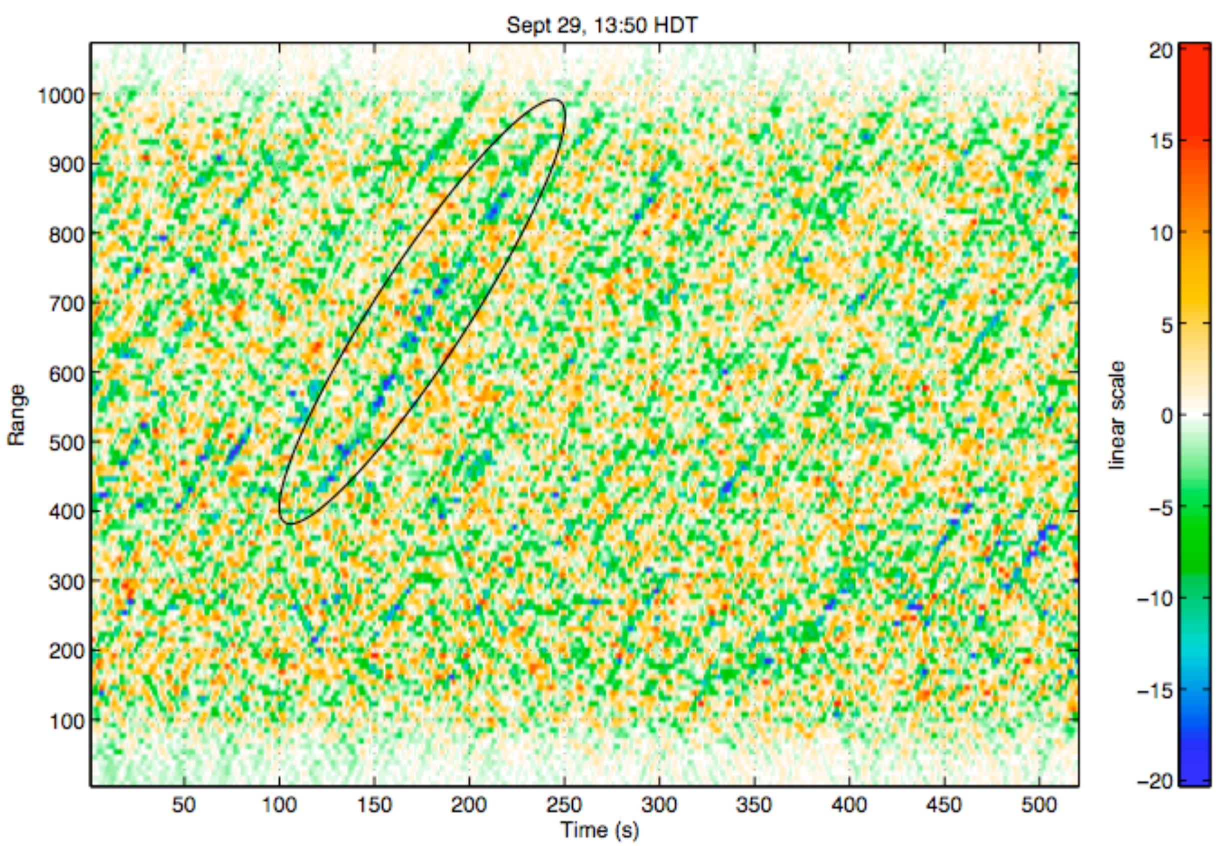

Figure 8. T-R plot of the filtered non-wave surface velocities over the same time-range intervals as figure 2. A blue-green slash appears matching the location of the persistent wave group as circled in Figure 2. This is a strong surface signature that indicates a forced response to a wave group that is especially steep and short. This response produces a distinctive ridge of high variance in the corresponding *k-f* spectrum along a straight line representing a roughly constant speed of 5 m/s speed away from FLIP.

7. Discussion

The study of Smith (2006a) was motivated by the occurrence of a distinctive "ridge" observed in the *k-f* spectra of surface velocities (as in Figure 4). The ridge appears along a line corresponding to about 5 m/s on the *k-f* plane. Smith (2006a) found that the physical location and strength of this Eulerian response corresponds well with that of the waves' Stokes drift, but is larger than predicted by theory. We defer speculation about possible causes of this large response, and focus on the response here only as a proxy for the occurrence of short steep wave groups. The coherence between Stokes drift and the Eulerian response was found by Smith (2006a) to be between –0.3 and –0.4, which is small but well above the 95% significance level. As discussed below, this low level of coherence is largely accounted for by the expected Doppler noise floor of the velocity estimates for the configuration of the deployment. Note that, consistent with the dynamics thought to play a part, this response emphasizes wave groups that are both steep and short. The 9 days analyzed in this way encompass the example shown, and have winds varying from 0 to 10 m/s.

Figure 8 shows the "non-wave" filtered surface velocities for the case discussed above. A significant "slash" of negative velocity (current towards FLIP) is located along the same line on the time-range plane as the short persistent surface wave group circled in figure 2, consistent with Smith's earlier finding (which was for a different data segment, on a different day, than that shown here).

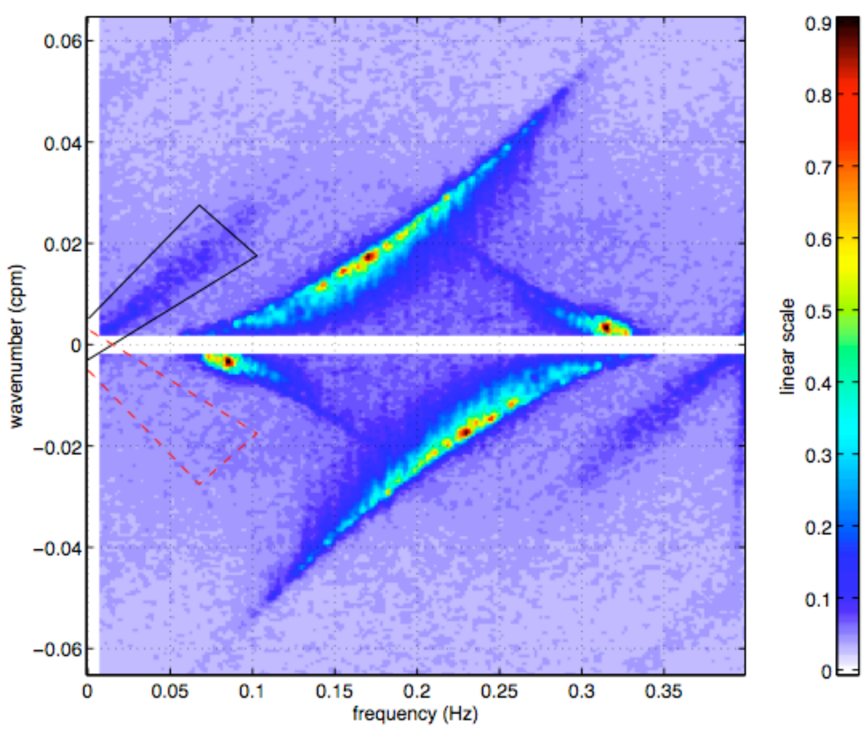

Figure 9. An example *k-f* spectrum showing the "5 m/s" masks. We focus on the region of the downwind-directed 5 m/s ridge ("D5," black outline) as a proxy for the strength of the forcing wave groups in comparison to the control case ("U5," red dashed), which selects upwind-directed responses, and is expected to reflect mainly the noise level of the spectral estimates. An especially strong group or several moderate ones may produce an equivalent signal in this way. This spectral response emphasizes groups that are steep, short, and persistent.

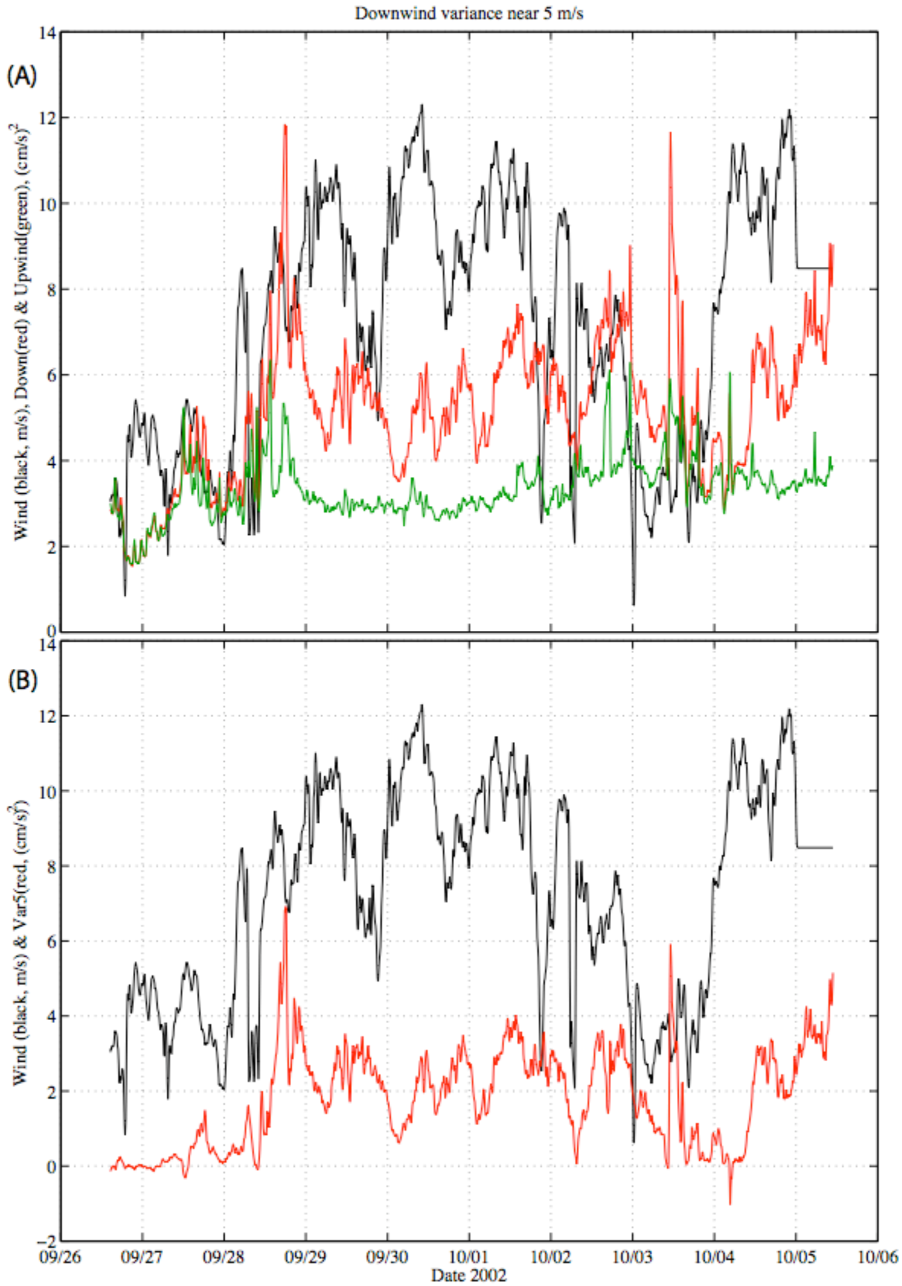

Figure 10. (Top) The wind (black), "downwind masked variance" (D5; red), and "upwind masked 5 m/s variance" (U5, green) over 9 days. At the start of this period, the wind had been calm, and both the D5 and U5 estimates are near the expected noise level. Shortly after the wind rises, the D5 variance increases more than U5 does. (Bottom) Wind (black) and the difference (D5-U5), thought to be a better indicator of just the signal portion of the "5 m/s" variance. Correspondence with the wind is better for the differenced result, with a delay of order ½ day. The highest peak in D5-U5 occurs early after the wind rises, on the evening of September 28.

To form a measure of the strength and/or frequency of occurrence of the compact persistent groups, we examine the variance along the 5 m/s ridge in *k-f* spectra formed from each 8.5 minute data segment. To estimate the "5 m/s variance," we mask the *k-f* spectrum over two separate 5 m/s bands, one going downwind (the proxy), and another going upwind (a "control," since we expect no such upwind-propagating groups). Figure 9 shows an example *k-f* spectrum with outlines of the two masks.

The downwind mask (D5) and upwind mask (U5) were applied to the sequence of data files from 1430 HDT September 26 to 1725 HDT October 4, 2002. The results (Figure 10) show D5 variances that correspond fairly well with the wind, fading to near the noise floor when the wind has been calm for a few hours, and rising shortly after the onset of 10 m/s winds. We also checked how these "proxy results" match a visual assessment from TR plots, and found the correspondence to be good.

Given the area of the masked region of the spectrum and the expected Doppler noise level, the estimated responses can be compared to the expected noise floor. The expected rms Doppler noise ΔV can be written in terms of the speed of sound c^s (≈1540 m/s), the center frequency f_0 (50 kHz), the sample interval τ_s (0.1 ms), the length of the repeat sequence code L (23 samples), the number of samples averaged in range N_a (100), and the number of "overlap samples" $(M\text{-}1)L$, where M (=9) is the number of code-repeats transmitted (Smith and Pinkel 1991):

$$\Delta V = \frac{c_s}{4\pi f_0 \tau_s}\left(\frac{1+N_a/2N_0}{LN_aN_0}\right)^{1/2} \approx 4.25 \text{ cm/s.} \tag{7.1}$$

Two further adjustments are needed: (1) in practice, the empirical noise variance is typically about double this value (increasing the rms by $2^{1/2}$), and (2) the received signal is filtered to 70% full bandwidth, which has the net effect of reducing L by a factor 0.7 in the above equation. The resulting adjusted estimate of the rms Doppler noise is 7.18 cm/s.

The D5 and U5 masks each capture about 1/25th of the total spectral area (actually 1331/32768), so the Doppler noise is expected to contribute about 2.1 $(\text{cm/s})^2$. As seen in Figure 10, this is consistent with both the D5 and U5 results over the first day or so, and then (as the wind rises), the "control" U5 increases to about 3, while the group-proxy D5 increases to between 4 and 7 $(\text{cm/s})^2$. Since some genuine surface activity is expected in the presence of wind, the indication is that the control U5 is a fair measure of the noise, and the difference D5-U5 is a good measure of the actual group-forced response signal, as desired.

Overall, the downwind 5 m/s variance (D5) increases to about 2 to 4 $(\text{cm/s})^2$ larger than the control (U5) as the wind increases (to about 10 m/s). A delay is also seen, on the order of ½ day between the wind rising and the response appearing. Two "spikes" are seen in the estimates, one near 1800 HDT on 26 September, and the other near noon on 3 October. Upon examination, the latter appears to be a result of some very loud ambient noise, while the former, on the evening of 28 September, represents an exceptional collection of short steep wave groups (see figure 11).

Finally, we re-consider the coherence levels observed by Smith (2006a) with the spectral noise level estimate in hand. The non-wave filter used in that analysis corresponds to about 2/3 of the spectral area (21972/32768), so the Doppler noise estimate yields a contribution of about 35 $(\text{cm/s})^2$, while the group-forced response estimate (D5-U5) for that example yields about 4 $(\text{cm/s})^2$. Thus, the maximum coherence magnitude possible, even if the 4 $(\text{cm/s})^2$ signal were perfectly correlated with the waves' Stokes drift, would be only $(4/39)^{1/2} = 0.32$, which is consistent with the reported result. Thus, it appears that the true signals (non-wave response and Stokes drift) must be very tightly correlated indeed.

The typical contribution to the 5 m/s downwind variance from the Eulerian responses in each data segment is about 3 $(cm/s)^2$, and the actual "slashes" have velocities of order 10 cm/s; thus, it appears that such a response is present about1/33rd of the time. Since the duration of the peak part of a group is on the order of one wave period (= 7 s), this would imply a group is typically encountered about once every 4 minutes or so. This is consistent with our visual estimate of 2 to 3 times per data segment (8.5 min); however, some segments have quite a few more (see figure 11!), while others have none.

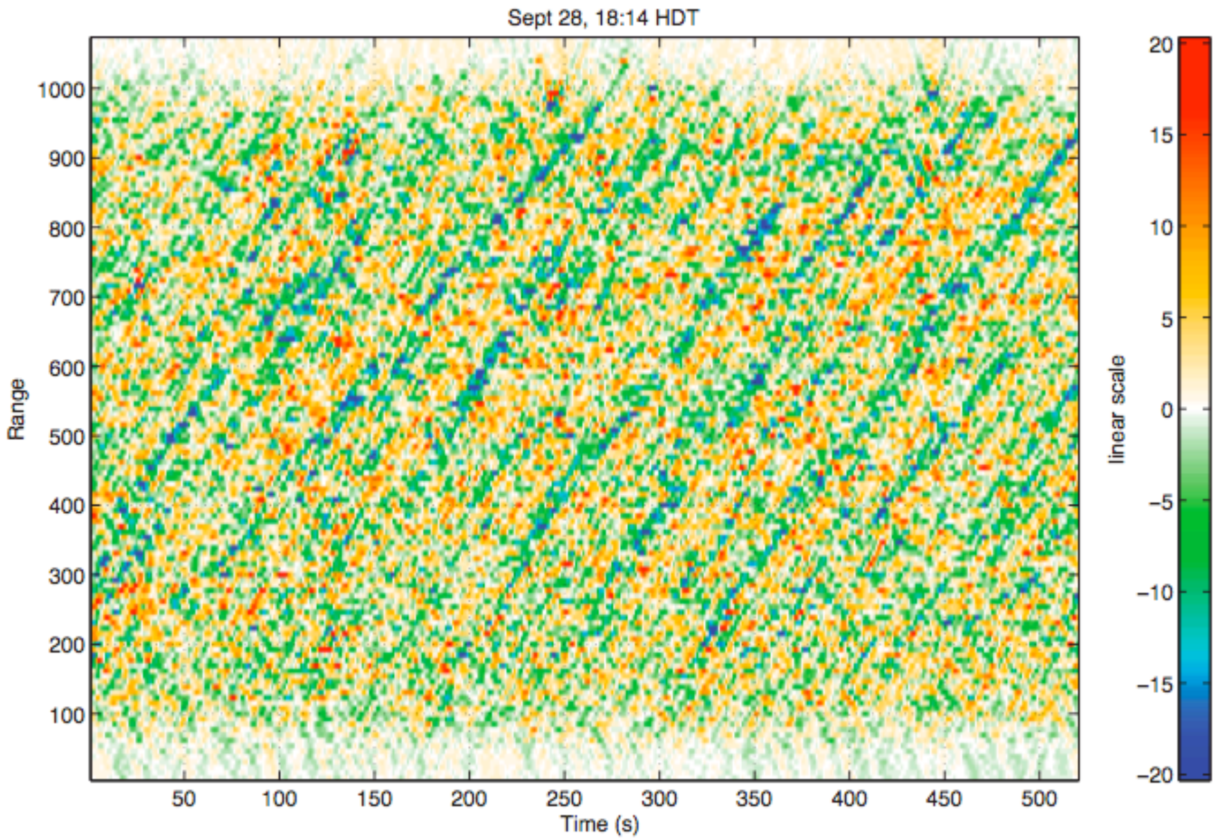

Figure 11. T-R plot of the non-wave filtered surface velocity for 1814 HDT 28 September. As indicated by the strength of the proxy measure (D5-U5), there are many strong "Eulerian group response" events. The corresponding wave-velocity T-R plot shows a corresponding number of short and steep wave groups, and so corroborates this interpretation (not shown for brevity).

8. Conclusions

Persistent wave groups propagating at about 5 m/s were observed to occur frequently over the several days considered, whenever there was a favorable wind. Linear propagation dynamics are sufficient to explain these observed groups. Very short "groups," only one wavelength long, can persist as long or even longer than those observed, up to 18 wave periods for the group envelope geometry observed. The key to this persistence is that the waves comprising the groups have crests oriented at an angle relative to the group envelope's major axis.

Using the previously noted Eulerian responses as a proxy for the existence of such short, steep, persistent wave groups, we attempted to assess how often they occur. Over the 9 days studied, winds rose from calm to 10 m/s twice. After the wind blows for a while, the downwind ridge has higher variance than the corresponding upwind ridge (which is hypothesized to be a measure of the noise level of the spectral estimates). The delay after the onset of wind is of order ½ day. The estimated Doppler noise levels are generally consistent with the assumption that the "upwind ridge" is a fair measure of the noise, with just a bit of additional environmental noise.

When the wind was blowing (~10 m/s), the compact persistent groups were encountered roughly 2 to 3 times per data segment (8.5 minutes), or 15 to 20 times per hour.

Acknowledgements. The field work and initial analysis was supported by ONR (N00014-02-1-0855); with additional analysis and modeling supported by NSF (OCE 06-23679). Thanks are due to the OPG engineering team of E. Slater, M. Goldin, M. Bui, A. Aja for their tireless efforts to design, construct, deploy, and operate the LRPADS and help develop the software to acquire and analyze the data, and to many others for many interesting and educational conversations.

References

Crawford, C. B., and D. M. Farmer, 1987: On the spatial distribution of ocean bubbles. J. Geophys. Res., 92, 8231-8243.

Dysthe, K. B., 1979: Note on a modification to the non-linear Schrodinger-Equation for application to deep-water waves. Proceedings of the Royal Society of London Series a-Mathematical Physical and Engineering Sciences, 369, 105-114.

Klymak, J. M., R. Pinkel, and L. Rainville, 2008: Direct breaking of the internal tide near topography: Kaena ridge, Hawaii. J Phys Oceanogr, 38, 380-399. doi:10.1175/2007jpo3728.1

Longuet-Higgins, M. S., 1978: Instabilities of gravity-waves of finite-amplitude in deep water. 2. Subharmonics. Proceedings of the Royal Society of London Series a-Mathematical Physical and Engineering Sciences, 360, 489-505.

Longuet-Higgins, M. S., and R. W. Stewart, 1962: Radiation stress and mass transport in gravity waves, with application to 'surf-beats'. J. Fluid Mech., 13, 481-504.

Pinkel, R., and J. A. Smith, 1992: Repeat-sequence coding for improved precision of Doppler sonar and sodar. J. Atmos. Oceanic Technol., 9, 149-163.

Pinkel, R., and D. Rudnick, 2006: Hawaii Ocean Mixing Experiment (HOME). J Phys Oceanogr, 36, 965-966.

Smith, J. A., 2002: Continuous time-space sampling of near-surface velocities using sound. J. Atmos. Oceanic Tech., 19, 1860-1872.

——, 2006a: Observed Variability of Ocean Wave Stokes Drift, and the Eulerian Response to Passing Groups. J. Phys. Oceanogr., 36, 1381-1402.

——, 2006b: Wave-Current Interactions in Finite Depth. J. Phys. Oceanogr., 36, 1403-1419.

——, 2008: Vorticity and divergence of surface velocities near shore. J. Phys. Oceanogr., 38, 1450-1468. doi:10.1175/2007/JPO3865.1

Smith, J. A., and R. Pinkel, 1991: Improvement of Doppler estimation through repeat sequence coding. Oceans '91/Proceedings, October 1-3, 1991, Honolulu, Hawaii, USA/Ocean Technologies and Opportunities in the Pacific for the 90's, IEEE, 977-984.

Smith, J. A., and G. T. Bullard, 1995: Directional surface wave estimates from Doppler sonar data. J Atmos Ocean Technol, 12, 617-632.

Thorpe, S. A., 1986: Bubble clouds: A review of their detection by sonar, of related models, and of how Kv may be determined. Oceanic Whitecaps and Their Role in Air-Sea Exchange Processes, E. C. M. a. G. M. Noicall, Ed., D. Reidel, 57-68.